Segmentation of spatial experience by hippocampal theta sequences

Anoopum S. Gupta
Matthijs A. A. van der Meer
David S. Touretzky
A. David Redish

Supplemental Information.

Nature Neuroscience: doi:10.1038/nn.3138

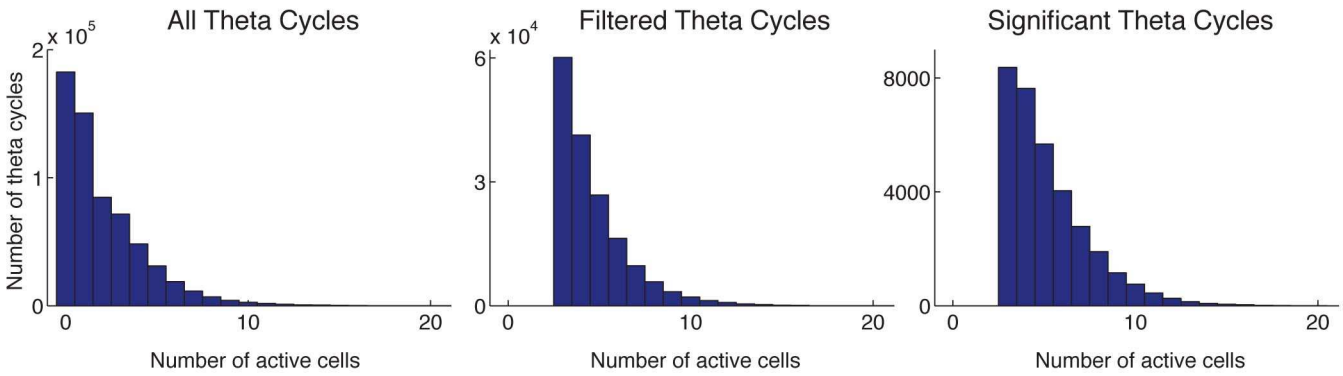

Figure S1: Histograms of the number of theta cycles versus the number of active cells per theta cycle. **Left** panel includes all theta cycles over 31 recording sessions (618,408 cycles). **Middle** panel includes theta cycles with three or more active cells, mean sharp wave ripple power less than one standard deviation above the mean, and theta power greater than one standard deviation below the mean (168,770 cycles). **Right** panel includes theta cycles whose neural activity contains significant sequential structure as described in the Experimental Procedures (33,397 cycles).

Nature Neuroscience: doi:10.1038/nn.3138

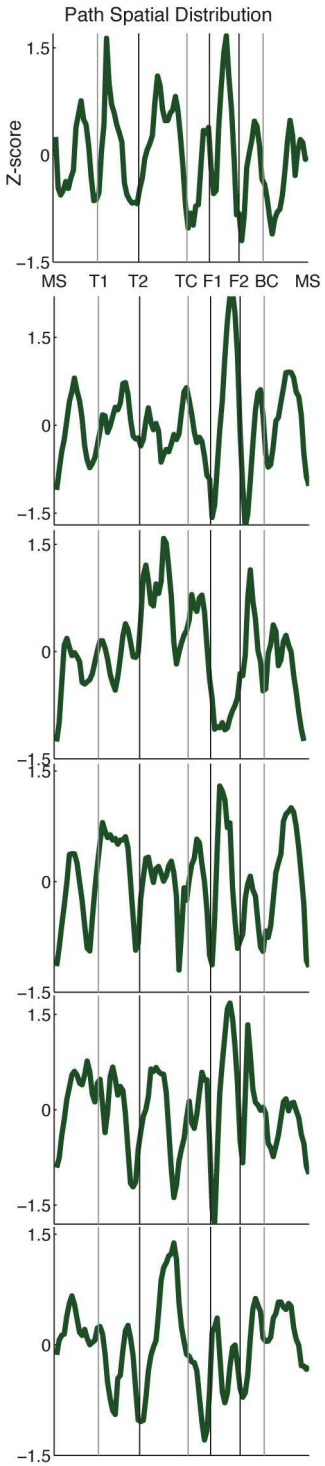

Figure S2: The distribution of space represented by theta sequences for each rat. The main results are robust across individual rats; all six rats chunked the behavior in similar ways.

Nature Neuroscience: doi:10.1038/nn.3138

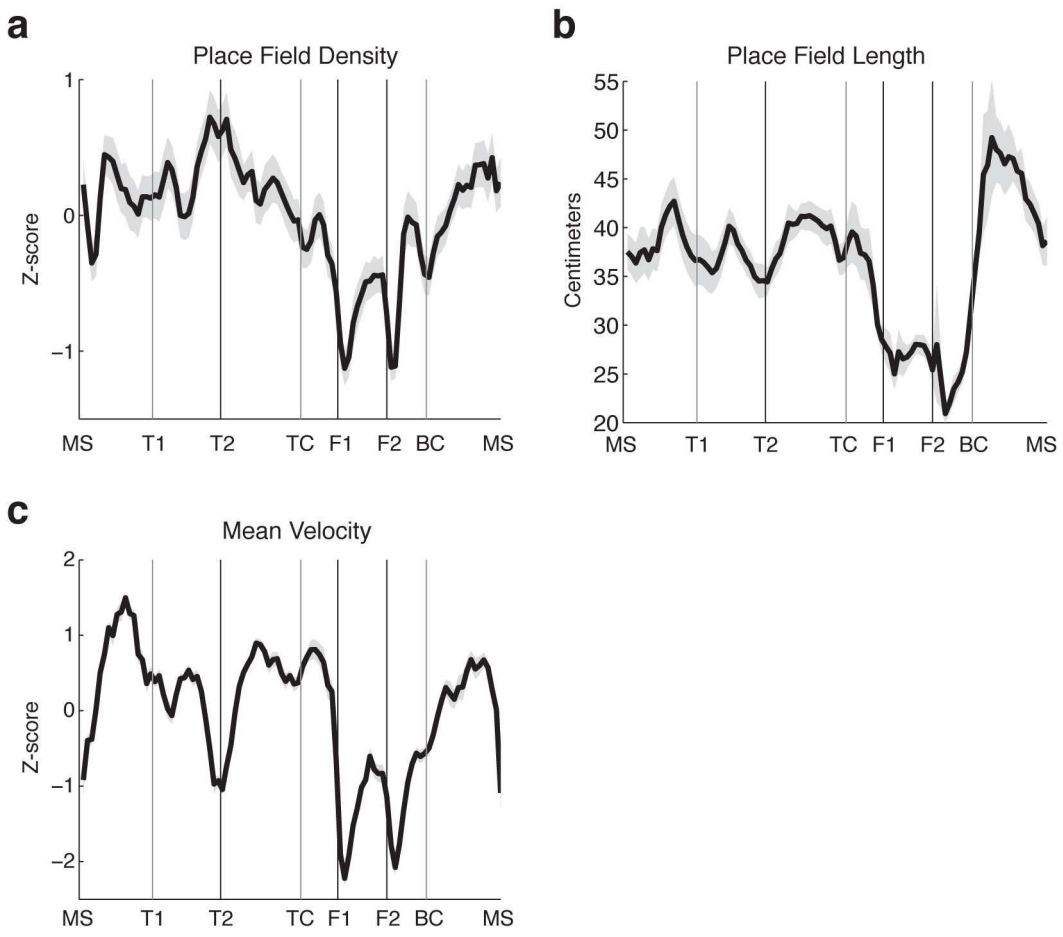

Figure S3: Relationship between place field density, place field length, and animal velocity, and location on maze. **(a)** Place field density as a function of location on linearized maze (n = 2,729 place fields). The height of the curve reflects the number of place fields overlapping a particular location in the environment. Y-axis is z-scored place field distribution by session, x-axis is linearized maze. **(b)** Mean place field length as a function of location. Place field length is defined as the length of the place field measured along the linearized maze. Y-axis is centimeters averaged by session, x-axis is linearized maze. **(c)** Animal velocity as a function of location on linearized maze. Y-axis is z-scored velocity by session, x-axis is linearized maze. Gray line width is s.e.m.

Nature Neuroscience: doi:10.1038/nn.3138

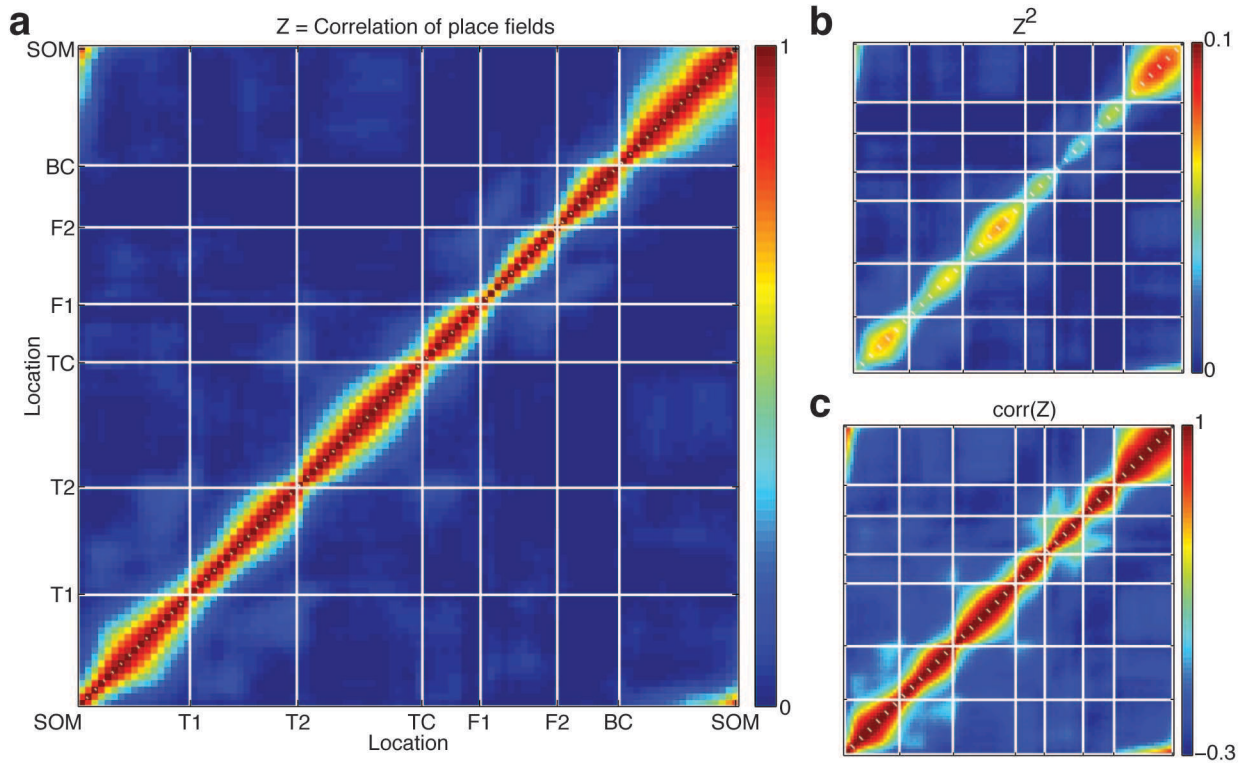

Figure S4: **(a)** Spatial correlation matrix of place fields. To calculate this matrix, the spatial firing tuning curve (place field) of each cell was calculated, creating an $n_{\text{cell}} \times n_{\text{spatial-bin}}$ matrix, with each element in the matrix the average firing rate of the cell at that particular location in the environment. This matrix was then correlated to create an $n_{\text{spatial-bin}} \times n_{\text{spatial-bin}}$ matrix. (**b**) The square of the matrix shown in panel **a**. (**c**) The cross-correlation of the matrix generated in panel **a**. 2,729 place fields were used in this analysis.

Nature Neuroscience: doi:10.1038/nn.3138

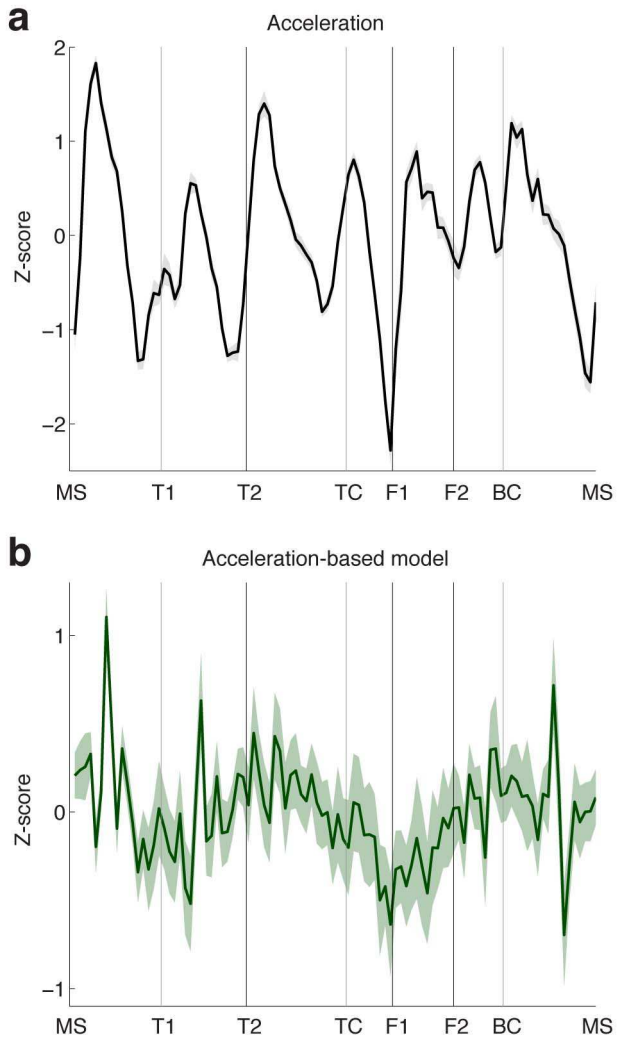

Figure S5: Spatial distribution of paths constructed from an acceleration-based model of represented spatial paths. **(a)** Mean acceleration (z-scored by session) as a function of location on linearized maze. **(b)** Spatial distribution of paths constructed based on the relationship between acceleration and ahead and behind length (see main text for details). Comparing this to the spatial distribution shown in **Figure 6** of the main text clearly shows that acceleration is not the sole driving force for spatial chunking. 29,351 theta sequences were used in this analysis. Line width is s.e.m.

Nature Neuroscience: doi:10.1038/nn.3138

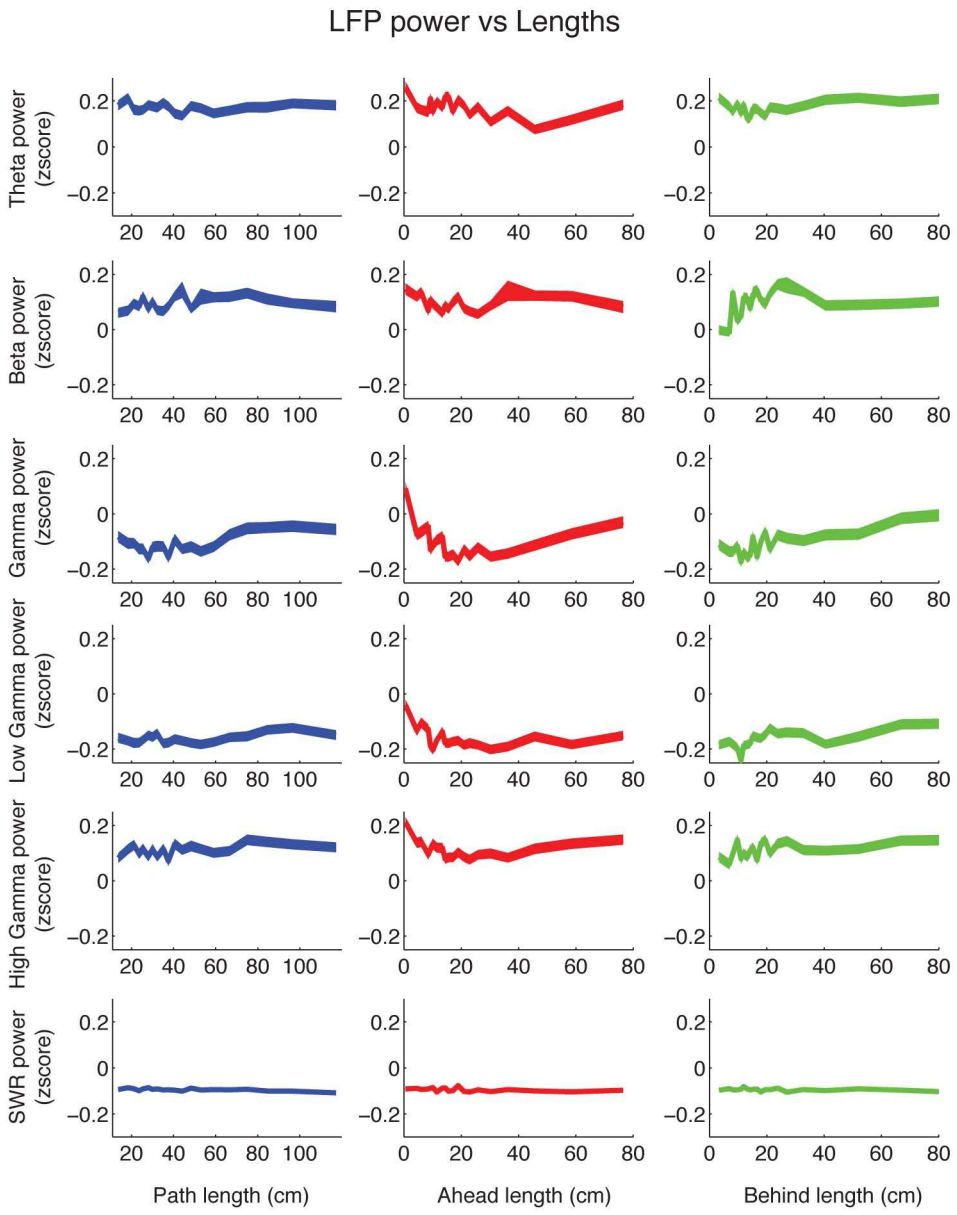

Figure S6: Mean LFP power as a function of path, ahead, and behind length. 29,351 theta cycles were used in this analysis. Mean LFP power was z-scored by session. Line width is s.e.m.

Nature Neuroscience: doi:10.1038/nn.3138

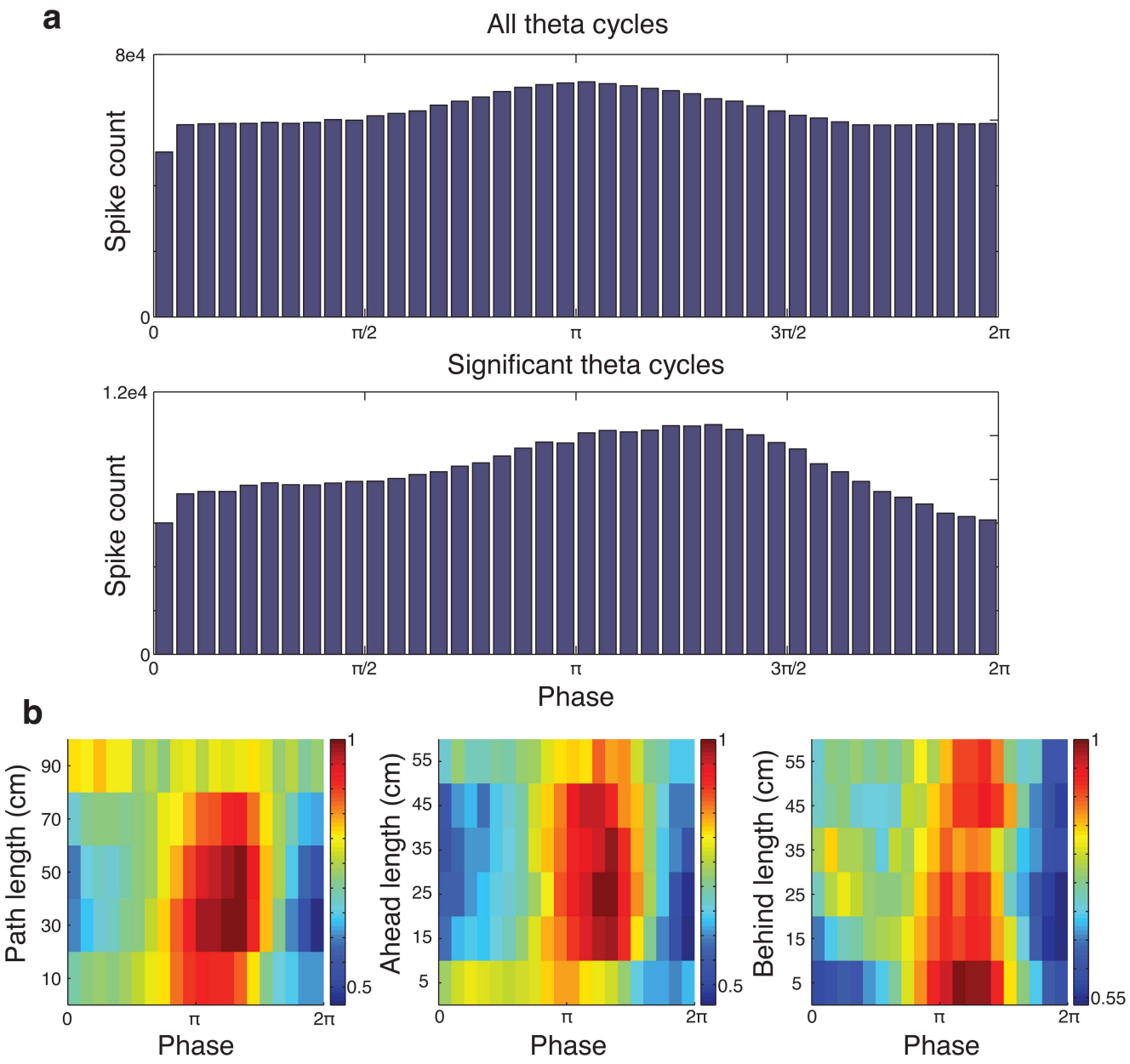

Figure S7: Theta sequence versus theta phase relationships. **(a)** Histogram of putative pyramidal cell spiking as a function of theta phase for all theta cycles **(top)** and for those theta cycles included in the analysis **(bottom)**. Minimal cell firing was observed at the peak of theta (0 and 2π). **(b)** 2D histograms showing the distribution of spikes over theta phase as path length **(left)**, ahead length **(middle)**, and behind length **(right)** increase. Red indicates high spike counts and blue is low spike counts. As seen in this figure, the distribution of spikes over the theta cycle is similar as the three lengths increase, and are similar to the distribution of spikes for all significant theta cycles (see panel

Nature Neuroscience: doi:10.1038/nn.3138

a). Note that the distribution of spikes over the theta cycle for the longest path lengths is based on relatively few theta cycles, which is the likely cause of the differing distribution. Phases of zero and 2π correspond to peaks of the theta oscillation recorded from the hippocampal fissure.

Nature Neuroscience: doi:10.1038/nn.3138

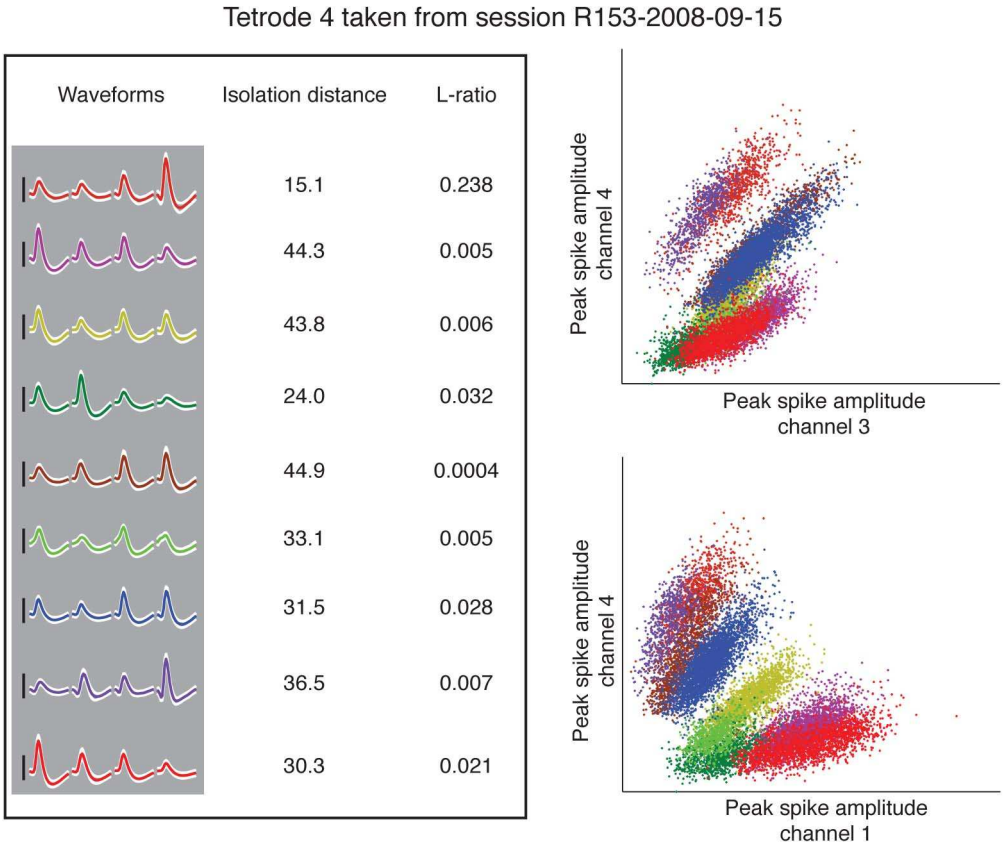

Figure S8: Example tetrode recordings from one recording session. Each spike cluster is shown with different colors on two projections (right). One millisecond waveforms for each of the four tetrode channels are plotted for each separable cluster along with the cluster's Isolation distance and L-ratio (left). Scale bar next to each cluster's waveforms is 100 μV.

Nature Neuroscience: doi:10.1038/nn.3138

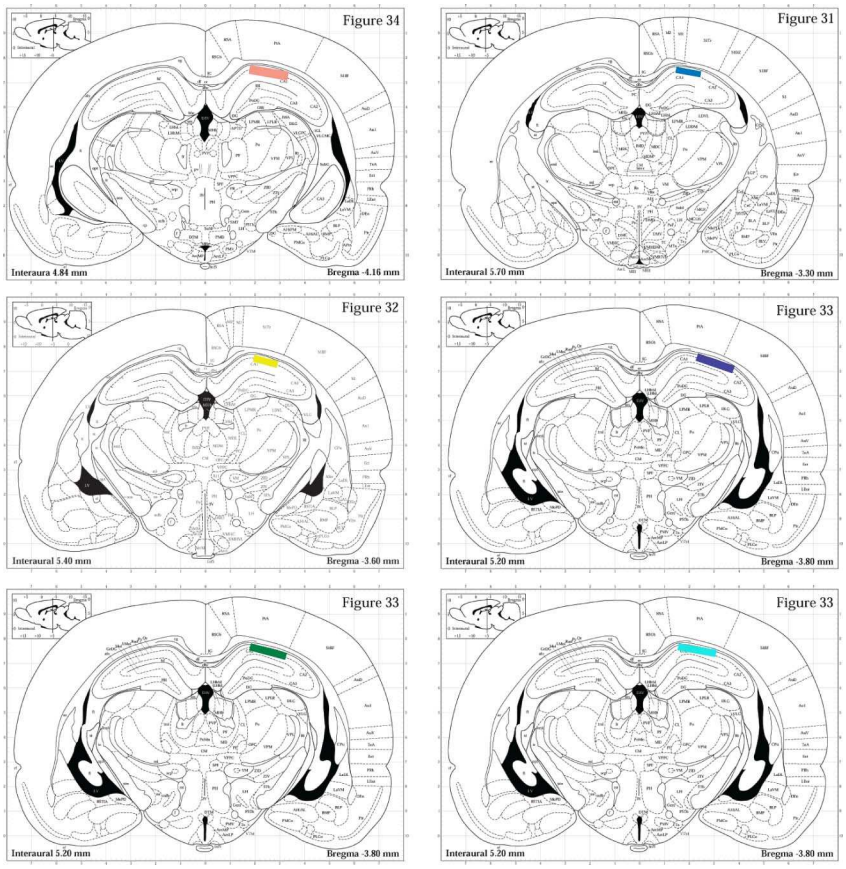

Figure S9: Schematics showing the position of implanted electrodes. Each colored box indicates the location of the electrodes within hippocampal region CA1 for each of the six rats in this study.

Nature Neuroscience: doi:10.1038/nn.3138